University of Texas at El Paso
DigitalCommons@UTEP

Open Access Theses & Dissertations

2016-01-01

Innovations In Thermoelectric Materials Research: Compound Agglomeration, Testing And Preselection

Hugo Lopez
University of Texas at El Paso, Hugo_lippmann@hotmail.com

Follow this and additional works at: https://digitalcommons.utep.edu/open_etd

 Part of the Condensed Matter Physics Commons

Recommended Citation
Lopez, Hugo, "Innovations In Thermoelectric Materials Research: Compound Agglomeration, Testing And Preselection" (2016). *Open Access Theses & Dissertations*. 882.
https://digitalcommons.utep.edu/open_etd/882

This is brought to you for free and open access by DigitalCommons@UTEP. It has been accepted for inclusion in Open Access Theses & Dissertations by an authorized administrator of DigitalCommons@UTEP. For more information, please contact lweber@utep.edu.

INNOVATIONS IN THERMOELECTRIC MATERIALS RESEARCH: COMPOUND AGGLOMERATION, TESTING AND PRESELECTION

HUGO FRANCISCO LOPEZ LOPEZ DE CARDENAS

Doctoral Program in Materials, Science and Engineering

APPROVED:

Russell R. Chianelli , Ph.D., Chair

Stephen W. Stafford , Ph.D.

Peter Golding , Ph.D.

Manuel Alvarado, Ph.D.

Charles Ambler, Ph.D.
Dean of the Graduate School

Copyright ©

by

Hugo Francisco Lopez Lopez De Cardenas

2016

Dedication

To my beloved son Ilan Matthias Lippmann Malterre.

INNOVATIONS IN THERMOELECTRIC MATERIALS RESEARCH: COMPOUND AGGLOMERATION, TESTING AND PRESELECTION

by

HUGO FRANCISCO LOPEZ LOPEZ DE CARDENAS, M.S.

DISSERTATION

Presented to the Faculty of the Graduate School of

The University of Texas at El Paso

in Partial Fulfillment

of the Requirements

for the Degree of

DOCTOR OF PHILOSOPHY

THE UNIVERSITY OF TEXAS AT EL PASO

May 2016

Acknowledgements

I would like to thank my wife, parents, and siblings for their support during these difficult years, I love you. My deepest gratitude goes to the “Becas y Programas en el Extranjero” scholarship program from the State of Chihuahua, Mexico for their economical support absolutely necessary to continue and finalize my doctoral studies. Thank you to my excellent friend Dr. Gabriel Gonzalez for his friendship, help, company, support, prayers and conversations. My most sincere expression of gratitude goes to Beatriz Tarango, administrative assistant of the Metallurgy and Materials Science department. Finally, I would like to thank the UTEP’s library for their excellent service.

Abstract

Thermoelectric materials have the capacity to convert a temperature differential into electrical power and vice versa. They will represent the next revolution in alternative energies once their efficiencies are enhanced so they can complement other forms of green energies that depend on sources other than a temperature differential.

Progress in materials science depends on the ability to discover new materials to eventually understand them and to finally improve their properties. The work presented here is aimed at dynamizing the screening of materials of thermoelectric interest. The results of this project will enable: theoretical preselection of thermoelectric compounds based on their bandgap and a rapid agglomeration method that does not require melting or sintering. A special interest will be given to Iodine-doped $TiSe_2$ that generated extraordinary results and a new set of equations are proposed to accurately describe the dependence of the power factor and the figure of merit on the intrinsic properties of the materials.

Table of Contents

List of Tables

List of Figures

List of Equations

Chapter 1: Introduction

Thermoelectrical generators (TEGs) directly convert a temperature differential into electrical current. The operation of these generators is completely noise and vibration free, while offering a non-intermittent production of electricity. While in service they do not produce emissions of any type and the generators do not require maintenance. The lifespan of the TEGs is on the order of decades and their use is usually limited by the availability of the temperature gradient.

The application of TEGs offers an entire new way to innovate, design and engineer new products and to improve current products. The versatility that this novel technology offers makes it applicable to almost every aspect of our everyday's life, civilian or military. The idea of harvesting electricity from waste heat is indeed a very attractive economically and environmentally. So far, the applications of TEGs for energy recovery have been limited, but the ever increasing demand for electricity pushes for innovation and new technologies.

But TEGs do not just work as electrical generators (Seebeck effect) when a temperature gradient is available, as they can also work as heating or cooling units (Peltier effect) when a voltage is applied. It is thanks to this dual working principle that makes TDs unique.

Fig. 1: TEGs dual working principle.

Chapter 2: Background

2.1 Historical developments

In 1821 Thomas Johann Seebeck discovered that if two different conductors are joined and the two junctions are maintained at different temperatures, an electromotive force is developed in the circuit. This principle now bears his name, the Seebeck effect.

Fig 2.1: Thomas Johann Seebeck.[1]

In 1834 Jean Charles Peltier was the first to observe and document that if a current flows in a circuit consisting of two different conductors then one of the junctions is heated and the other is cooled. This effect is now known as the Seebeck effect.

Fig 2.2: Jean Charles Peltier.[2]

An in-depth historical review of thermoelectric models had to be performed in order to understand the current standing of research in thermoelectrics. For the purposes sought here, key developments took place:

1821 Seebeck discovers the thermoelectric effect.[3]

1834 Peltier discovers the Peltier effect.[2]

1912 Altenkirch develops the concept of figure of merit (Z).[4,5]

1920's Abram Fedorovich Ioffe, a Soviet scientist proposed that semiconductors would make good thermoelectrics.[6]

1954 Goldsmid discovers Bismuth Telluride, a layered chalcogenide semiconductor and the best performing room temperature thermoelectric material to date.[7]

1959 Chasmar and Stratton[8] looked for an optimum gap of a thermoelectric semiconductor in order to optimize zT. They found that the best gap was $\approx 6k_BT$.

1962 Simon shows that very high zT values could be obtained in small bandgap semiconductors.[9]

1994 Sofo and Mahan[10] expanded Chasmar and Stratton's previous work by setting an optimal band gap range of $6k_BT$ - $10k_BT$.

2008 Snyder and Toberer[11] developed a model based on Bi_2Te_3 that shows the relationship between α, σ, k, PF, and *Z* in function of the carrier concentration. They state that good thermoelectric materials are typically semiconductors with a carrier concentration between 10^{19} and 10^{21} carriers per cm^3.

2013 Goldsmid states a material that fulfills the correct conditions might have a $zT \approx 6$. Such statement breaks with the paradigm that figures of merit above 2 for room temperature thermoelectric materials might not be achieved.[12]

2013 Lebègue *et al.* used data filtering and density-functional-theory calculations to screen selected layered chalcogenides out of the entire ICSD database in an effort to discover new semiconductors for general electronic applications.[13]

2.2 Seebeck modules and their applications

The basic building blocks of a modern Seebeck module (also known as Thermoelectric generator) are alternated p-type and n-type single-crystal Bismuth telluride-based semiconductors. If you apply current you will get a hot side and a cold side, on the other hand, if you apply heat on one side and cold on the other you will obtain electricity.

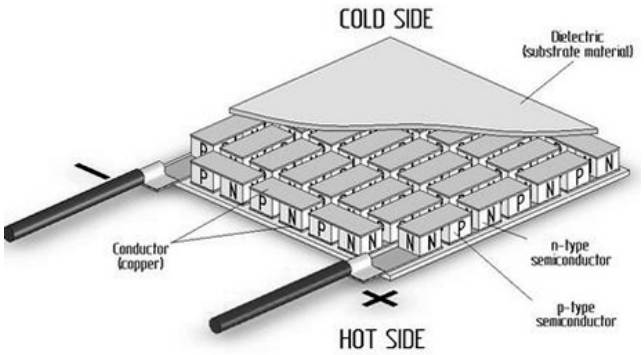

Fig. 2.3: Cross-sectional view of a Seebeck module.[14]

In 1953, the soviet radio manufacturer Metallamp developed a commercially available thermoelectrical generator as part of one of their quinquenal plans aimed to effectively use domestic resources. The TGK-3 thermoelectric generator supplied 2 – 5 W thanks to its ZnSb/constantan thermoelectric elements, enough to power a radio.

Fig.. 2.4: Soviet TGK-3 thermoelectric generator.[15]

The latest and probably the most common application for Thermoelectric generators (TEG) is found in electric wine cellars, which run on the most common thermoelements commercially available made of Bi_2Te_3. The advantages of this cellars when compared to conventional gas-refrigerated units are: 1) noiseless operation as there are no moving parts, 2) there is no vibration, 3) they provide a long service life, 4) lightweight, and 5) do not contain harmful gases.

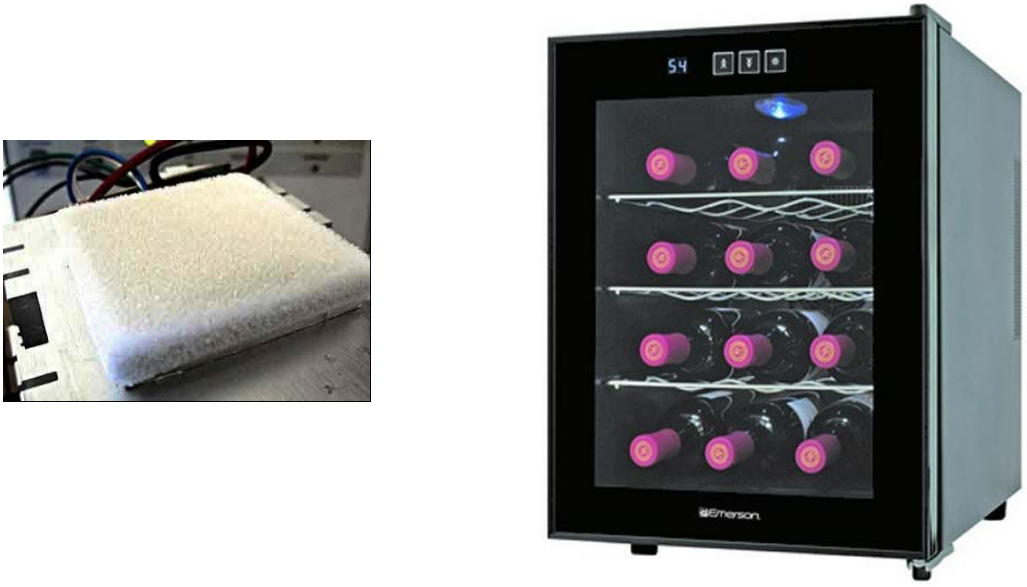

Fig. 2.5: *Left Image* Operating Peltier thermocooler on top of heat diffuser covered with ice, *Right Image* Emerson FR966 12 bottle wine cellar.

In 1998 Seiko Instruments Inc. (SII) commercialized the smallest TEG ever manufactured, and introduced the first application of TEGs into a watch. The success that SII had on miniaturizing TEG technology in order to make it wearable, earned the Seiko Thermic a place at the Smithsonian. The images below show on the left the Seiko Thermic watch,[16] and on the middle the conceptual figure of the thermoelectric-powered wristwatch. The backlid (high temperature end) receives heat from the wearer's arm effectively while the clock case (low-temperature end) radiates heat efficiently. Finally, the image on the right an electronic scanning electron microscope (SEM) photomicrograph is shown of the thermoelectric device used in the THERMIC. Contained in this device are 104 component elements each measuring 80x80x600-micrometers.[17]

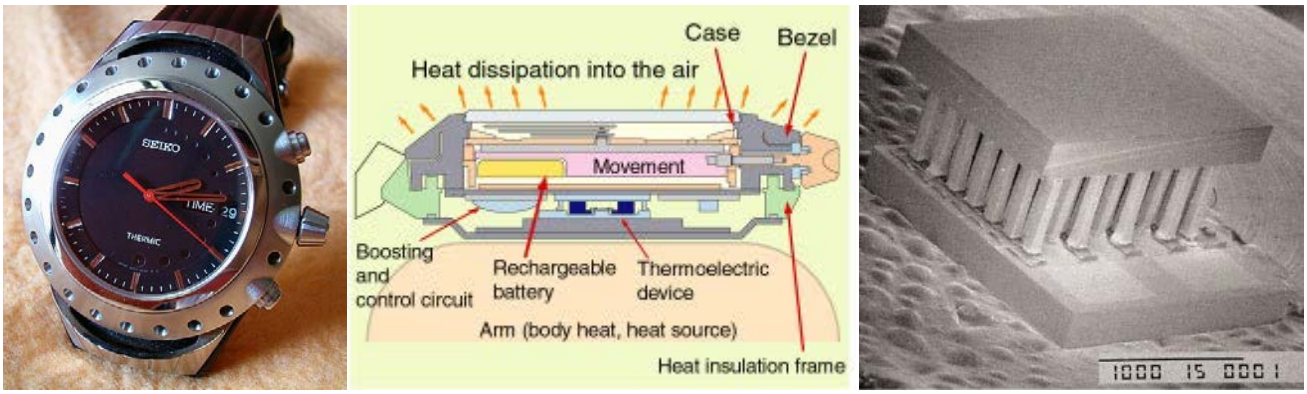

Fig. 2.6: *Left Image* Seiko THERMIC watch, [16] *Middle Image* The conceptual figure of the thermoelectric-powered wristwatch. *Right Image* SEM photomicrograph of the THERMIC TEG.

But then NASA wants to push further the miniaturization, and the Ames Research Center is currently developing TEGs that can be implanted subdermically. Such device would be used to power vital sign monitoring sensors or to recharge nanodevices.

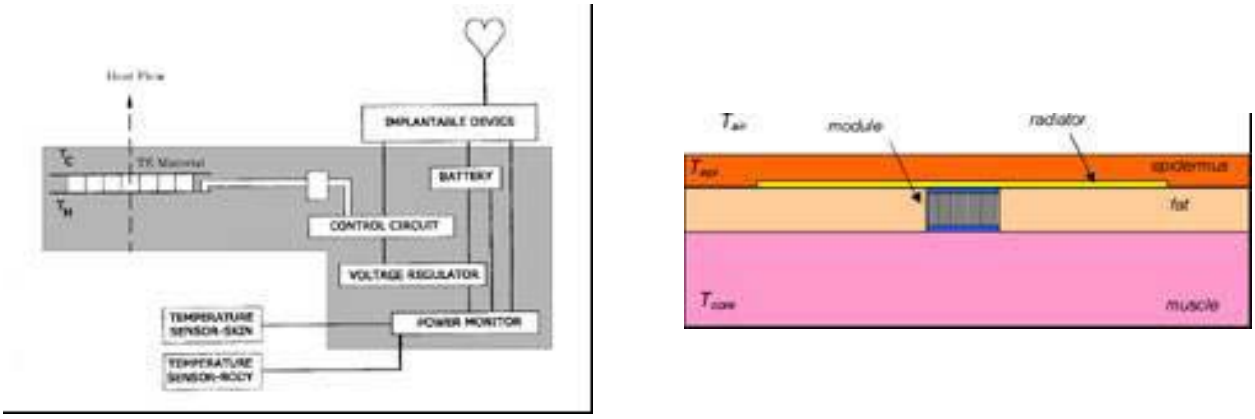

Fig. 2.7: *Left Image* Schematic block diagram circuitry for pacemaker battery, *Right Image* Schematic depicting a thermoelectric device to be implanted subdermally.[18]

TEGs have attracted the interest for military and space applications thanks to their capacity to generate electricity on practically any sort of environment once a thermal source is provided.

The Partisan's canteen was probably the first practical application of a TEG ever. It was developed by the soviets during the WWII, the pot at the bottom contained thermoelectric couples made of ZnSb (composite semiconductor) and constantan (Cu Ni alloy) that powered a radio under the heat of a fire camp.

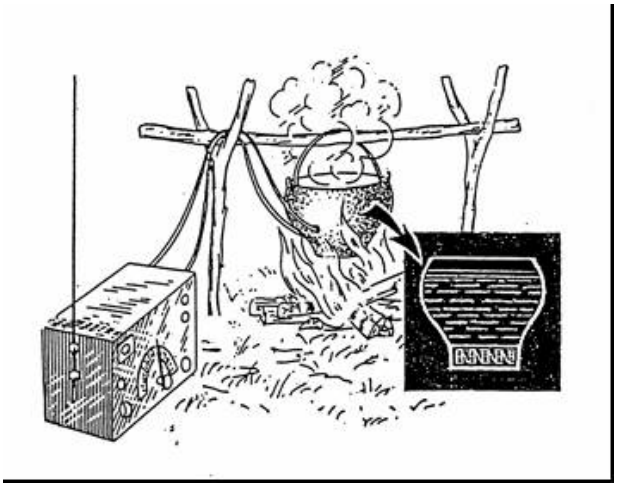

Fig. 2.8: Partisan's Canteen: thermoelectric generation by campfire (ZnSb/constantan thermo-elements).[19]

In the 1970's, the US developed a thermoelectric battery charger for the Army. It could run basically on all kinds of liquid fossil fuel (gasoline, jet fuel and diesel fuel) and it had an efficiency of approximately 3% thanks to their Lead Telluride (PbTe) thermo-element.

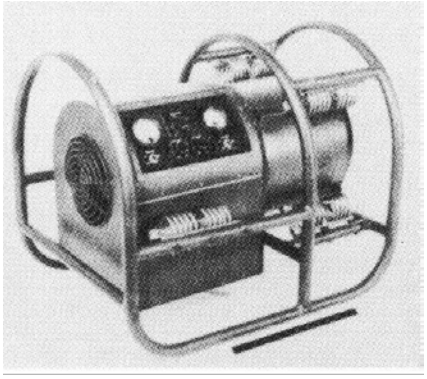

Fig. 2.9: American 500W portable generator using liquid fuel.[19]

Radioisotope Thermoelectric Generators (RTG) use thermo-elements that convert the decay heat of Pu-238 to electric power with system efficiencies that range from 5 – 7 %. Due to the versatility of RTGs, they have found applications in the most extreme of environments, including underwater espionage.

In 1979 the USS Parche submarine during Operation Ivy Bells installed an RTG-powered cable tapping pod was laid off in the Murmansk, in the Barents's sea. The tapping pods were not limited by their capacity to produce electricity, but rather because of their data storage capacity which lasted for up to a year.[20]

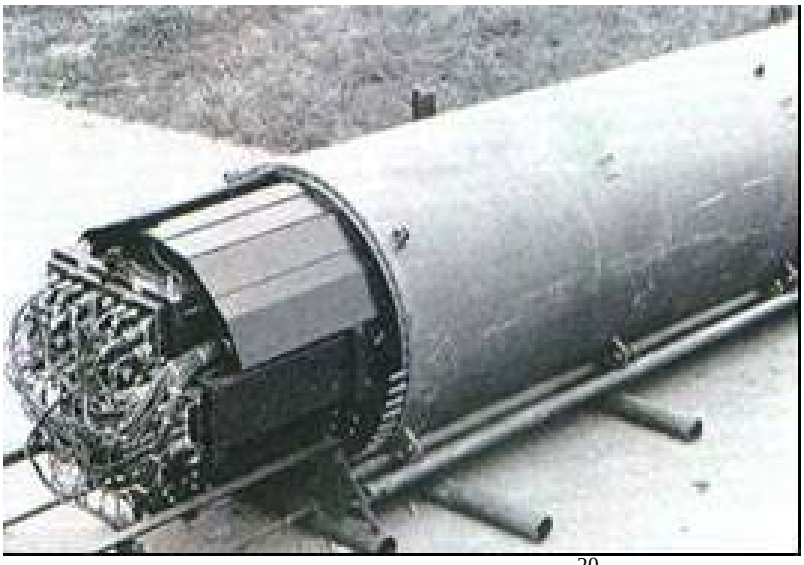

Fig. 2.10: The Ivy Bells device.[20]

Where solar panels cannot be used due to the absence of solar light, NASA has utilized RTGs. Up until now NASA claims that since 1961, 28 U.S. space missions have safely flown radioisotope energy sources.[21]

The heat source radioisotopic fuel is Plutonium-238 in the form of the oxide $Pu0_2$. In the isotopic decay process, alpha particles are released which bombard the inner surface of the container.[22] The energy released is converted to heat and is the source of heat to the thermoelectric converter.

This technology has been implemented on all of its radioisotope power systems (RPS) to provide electric power to both Viking landers, pioneer 10 and 11, voyager 1 and 2, the Cassini-Huygens mission to Saturn, and the new horizons mission to Pluto among others.[23]

Continuous research and development in the TEG field will result in lower-cost and higher efficiency devices. A higher efficiency on TEGs will directly translate into smaller and lighter devices which is critical for space missions and military operations.

Fig. 2.11: Cassini spacecraft RTG roughly the size of a person.[24]

The modern soldier depends now more than ever on electronic equipment for a successful task accomplishment. More efficient TEGs would enable the soldier to generate the required electricity to power small scale electronics by carrying a portable generator in its backpack. Such device would reduce the dependency on batteries and thus reducing the load to carry.

Furthermore, military underwear and space suits of the future could incorporate TGs to either cool-down or warm up the individual, and when not required it could be used to generate electricity to power or recharge their systems.

Rockets could be another application for TEGs. The large temperature gradient between the tip of the rocket and the exhaust nozzle could be used to reduce the load, the size and the weight of the batteries that power on-board systems. Such system would take advantage of the thermal work capacity of the combusted propellant once it has performed mechanical work increasing the overall efficiency of the device.

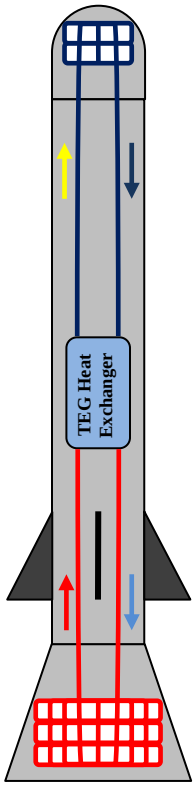

Fig. 2.12 Rocket with TEG-assisted electrical system.

There is also room for the implementation of TEGs in civil engineering. Building design and construction has evolved greatly over the last 60 years as: 1) new materials are available, 2) greater importance to aesthetics is given, 3) an effort to minimize operational energy consumption. The design of new buildings is undergoing a transitional period in terms of operational energy consumption from

self-sustainability to positive. This means, that energy (electricity in this case) will be generated in excess within the building so it can be in turn reintegrated to the municipal power grid.

Negative Minimize Sustainable Positive

Fig.. 2.13: Evolution of operational energy consumption in buildings.

Such is the case of the Masdar headquarters, world's first positive energy building in the new city of Masdar in the United Arab Emirates.[25]

Fig. 2.14: Masdar headquarters, world's first positive energy building in Masdar Abu Dhabi, UAE.[25]

Passive and dynamic solar systems play a big role in this new tendency, a tendency that has pushed the implementation of photovoltaic cell arrays to its maximum and has neglected totally thermoelectrical generation.

Thermal gradients can be found everywhere in a building, i.e. heat is released from the decomposing matter in the sewage system, incoming municipal water, and from windows like those that BASF™ designed for the new buildings in Masdar city.

The following drawing shows a simple sun heated water (or sewage) -cold air heat exchanger or radiator which could be used during winter times or cold regions. Hotter exiting hot air could be used for HVAC purposes.

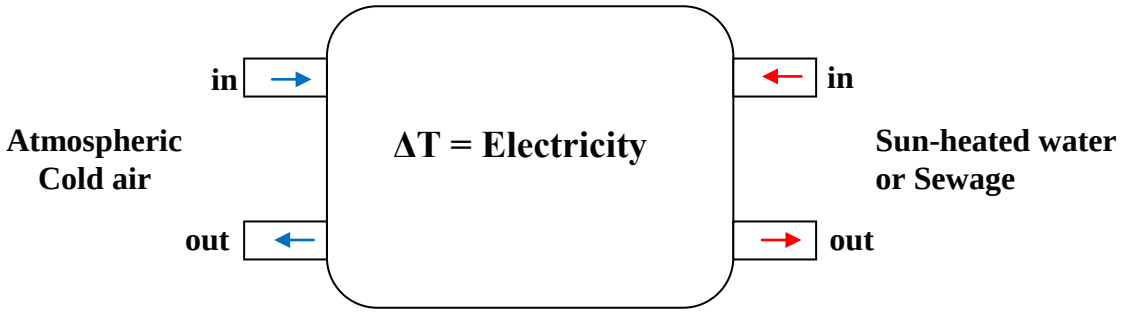

Fig. 2.15: Sun heated water or sewage-cold air heat exchanger.

The same concept could be used for hot regions, using relatively cold water incoming from the municipal distribution system and atmospheric hot air. Outgoing air would be relatively at a lower temperature (vs. incoming) and could be used for HVAC purposes as well.

The revolutionary windows that BASF™ designed for Masdar are based on the concept of integrating a heat exchanger and a window in a single component, so the window works as a heat pump:

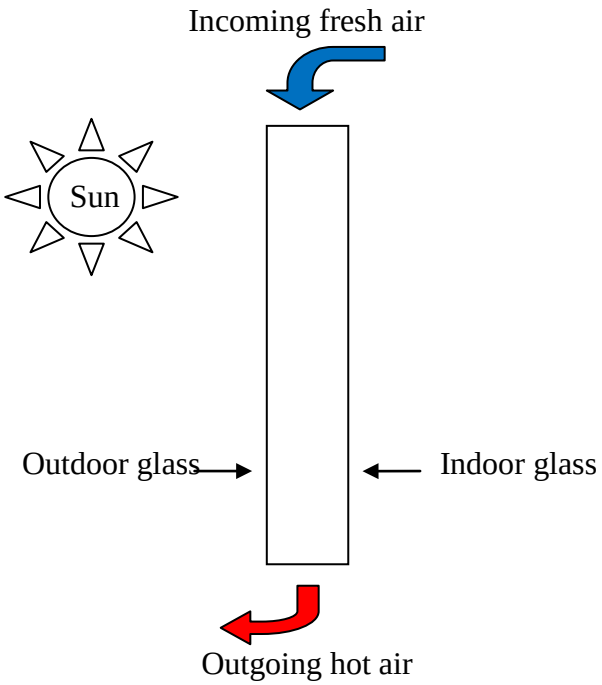

Fig. 2.16: BASF™ windows for Masdar city.

The product developed by BASF™ will lower HVAC-related energy costs by at least 30% according to the manufacturer. A similar window concept lined with TEGs could be used not just generate electricity but could be used also supply HVAC requirements if an electrical current is applied.

The use of TEGs can be very well complemented by other technologies; these can be solar, wind, geothermic or nuclear. For example, geothermal electrical generation works basically like any other conventional thermoelectrical generation powerplant, where cold water is turned into steam which is then used to power a turbine. Once the steam passes through the turbine and mechanical work is performed, the vapor is expelled. But even after the water vapor has performed the mechanical work, it still has the capacity to perform thermal work while it cools down to finally condense. The thermal work capacity can be exploited via TEGs means like the following diagram shows:

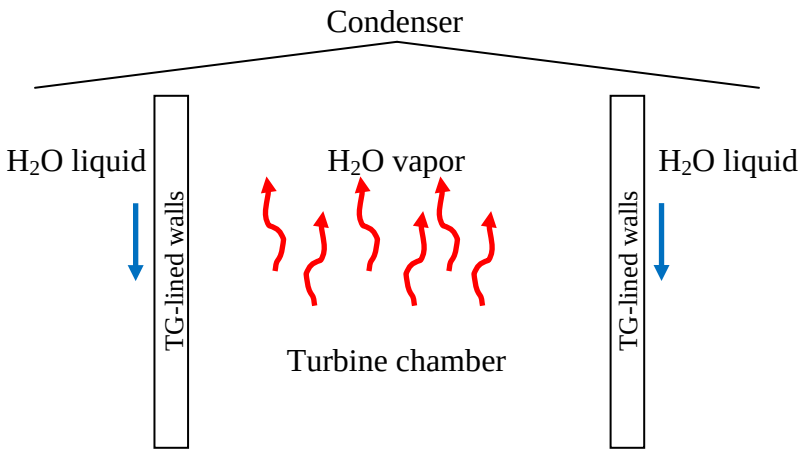

Fig. 2.17: Recovering thermal energy from water vapor in a thermoelectrical generation plant.

Thermoelectrical cooling and heating could be implemented in the auto industry, since the advantages that such a system would have over conventional systems are:

- Low weight, since heating and cooling systems are reduced to one system.
- Solid state device, no moving parts and no vibrations.
- Long service lifetime and no components subject to corrosion.
- No mechanical load on engine.
- No pressurized hot water or pressurized refrigerant.
- No risk of hot water entering the passenger cabin due to heater malfunction.

In 1954 Komatsu developed a thermoelectric air conditioner for the company's president vehicle, a Chrysler. Although the technology was never commercialized it was a breakthrough in thermoelectric applications.[26]

Fig. 2.18: Komatsu's Automotive Thermoelectrical A/C prototype.[26]

Automotive thermoelectrical generation has also been explored, but hasn't reached the market either. In 1999, the Clarkson University in Postdam in N.Y. and Delphi Corporation in Lockport N.Y. designed, fabricated and tested an automobile exhaust thermoelectric generator in a light truck. The generator was called AETEG, for "Automobile Exhaust Thermoelectric Generator", and the purpose of the generator was to improve vehicle's fuel economy and reduce its emission by converting waste exhaust energy so that the load on the vehicles alternator could be reduced.[27] The German automakers VW and BMW are currently exploring similar applications.[28]

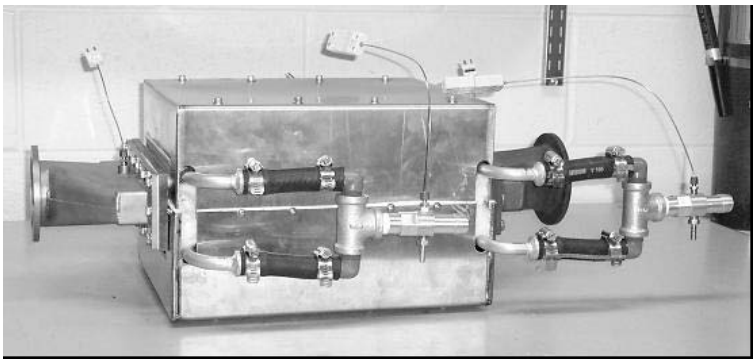

Fig. 2.19: Automobile Exhaust Thermoelectric Generator.[27]

2.3 Intrisic properties, power factor and figure of merit

The intrinsic properties that define a thermoelectric are the Seebeck coefficient (α), the electrical conductivity (σ) and the thermal conductivity (k). They are all condensed into one value that is the figure of merit (z):

$$z = \frac{\alpha^2 \sigma}{k}$$

Equation 2.1: Figure of Merit

The numerator is a useful parameter in assessing the performance of a thermoelectric, and it is termed as the Power Factor. Under a given temperature difference, the ability of a material to produce useful electrical power is quantified by its power factor (PF). Materials with high power factor are able to generate more energy in a space-constrained application.

$$PF = \alpha^2 \sigma$$

Equation 2.2: Power Factor

Sometimes z might be multiplied by the temperature in order to obtain a dimensionless figure of merit (zT):

$$zT = \frac{\alpha^2 \sigma\, T}{k}$$

Equation 2.3: Dimensionless Figure of Merit

Snyder and Toberer developed a model based on Bi_2Te_3 that shows the impact of the intrinsic properties (α, σ, k) on the PF and the zT in function of the carrier concentration.[29]

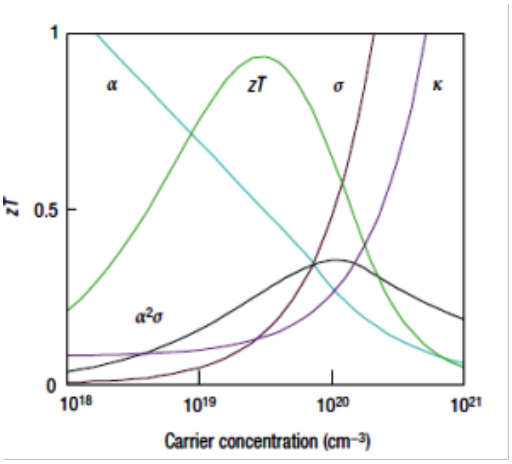

Fig. 2.20: *zT* and PF in function of *α, σ* and *k* for Bi_2Te_3.[29]

2.4 Compound Synthesis and Agglomeration

2.4.1 Chemical vapor transport (CVT)

Chemical vapor transport (CVT) is a relatively inexpensive technique and the standard method to grow crystalline bulk transition metal chalcogenides.[30] The starting materials for the crystal growth are filled with stoichiometric composition (A and B) in their solid condition (s) into a quartz ampoule together with a gaseous transport agent (L_g).

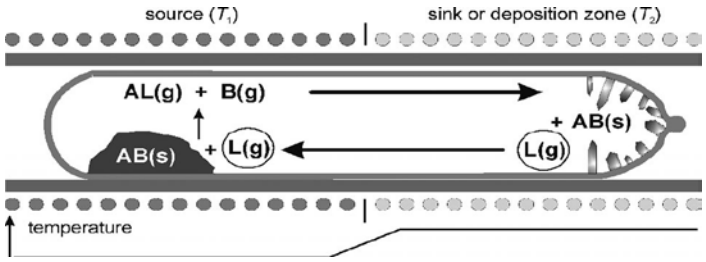

Fig. 2.21 Schematic of the CVT process.[31]

The ampoule is introduced into a furnace with a temperature gradient, source T_1 (hotter) and T_2 sink or deposition zone (cooler). The starting materials will form the gases $AL_{(g)}$ and $B_{(g)}$ in T_1 and will react in the cooler part T_2 growing crystalline bulk. The method generates small but highly pure polycrystals which can be later agglomerated to larger crystals via different methods, two of them being

the Bridgman method and the sintered uniaxial pressing. The work presented here presents the results of a novel agglomeration method: the unsintered uniaxial dry cold pressing .

2.4.2 The Bridgman Method

The Bridgman method is used to produce certain semiconductor crystals such as Gallium arsenide, II-V, II–VI (ZnSe, CdS, CdTe, and ZnTe), BGO ($Bi_4Ge_3O_{12}$ -Bismuth germanate-) [32-34] and Bismuth telluride (a V–VI compound).[35] It is a popular technique, because of the simplicity of the growth apparatus, the high growth rate and the availability of crystals of appropriate size and quality.[32]

It is one of the solidification methods developed to grow single crystal ingots or boules of semiconductors, but can be used for solidifying polycrystalline ingots as well.[36] Moreover, since it involves directional freezing, it will lead to a controlled distribution of impurities and to any preferred orientation.[37]

The Bridgman technique requires melting the raw polycrystalline material in a mold (ampoule or crucible) of smooth graphite, tapered to a point at the bottom end. Using a growth process called the gradient freezing (GF) method; a temperature gradient is applied along the length of the mold so that the temperature around the seed crystal is below the melting point.

The mold can be positioned either horizontally or vertically to control convection flow, being the most common the vertical arrangement. As the seed crystal grows, the temperature profile is translated along the mold by controlling the heaters along the furnace or by slowly moving the ampoule containing the seed crystal within the furnace.[38] When seed crystals are not employed as described above, polycrystalline ingots can be produced from a feedstock consisting of rods, chunks, or any irregularly shaped pieces once they are melted and allowed to resolidify. The resultant microstructures of the ingots so obtained are characteristic of directionally solidified metals and alloys with their aligned grains.[36]

The following schematic diagram graphically describes how the Bridgman method works:

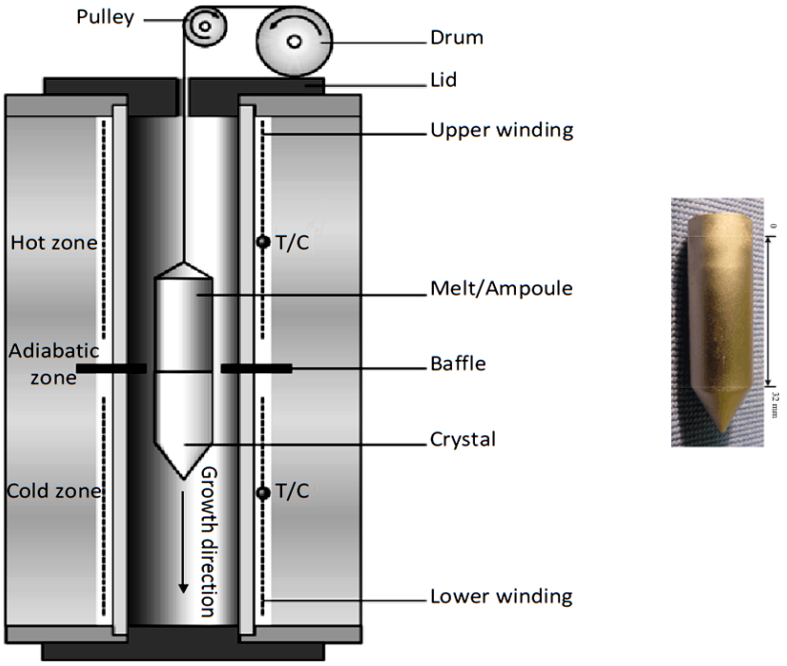

Fig. 2.22: *Left Image* Schematic of vertical Bridgman crystal growth furnace. Modified after 39 and 41. *Righ Image* Boule of a CuAlNi alloy grown by the Bridgman method.[7]

2.4.2.1 The Bridgman-Stockbarger method

The Bridgman-Stockbarger method is a variant of the Bridgman method, and often the arrangement is horizontal, with the charge held in a pointed boat (Fig. 2.23). This variant has the advantage that it does not require a seeded mold to initiate growth.[41]

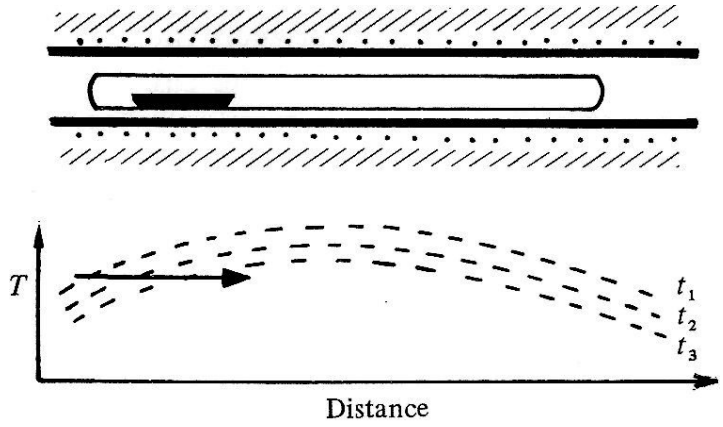

Fig. 2.23: Schematic of the horizontal Bridgman-Stockbarger method.[41]

There are number inconvenients inherent to this technique: post machining is required to obtain desired size and shape of samples, there is product adhesion to the crucible, crucible wall-induced stresses are created as well as large thermal strains introduced as the crystal cools. By far the most important disadvantages are those that induce property variations: introduction of impurities due to the high temperature contact –and contamination- with the crucible and stoichiometrical deviations due to preferential melt element diffusion into the crucible.

2.4.3 Uniaxial dry–cold pressing

Uniaxial dry–cold pressing (UDCP) is a high-pressure agglomeration in confined spaces technique. When compared to other agglomeration and compacting methods it is the simplest and least expensive of all, since all the equipment required is a hydraulic press and a rigid dry-pressing die set.

In UDCP, pressure is applied to the powder with a punch that displaces vertically, pressing, compacting and densifying the particulate mass contained in the rigid die (Fig. 2.24).

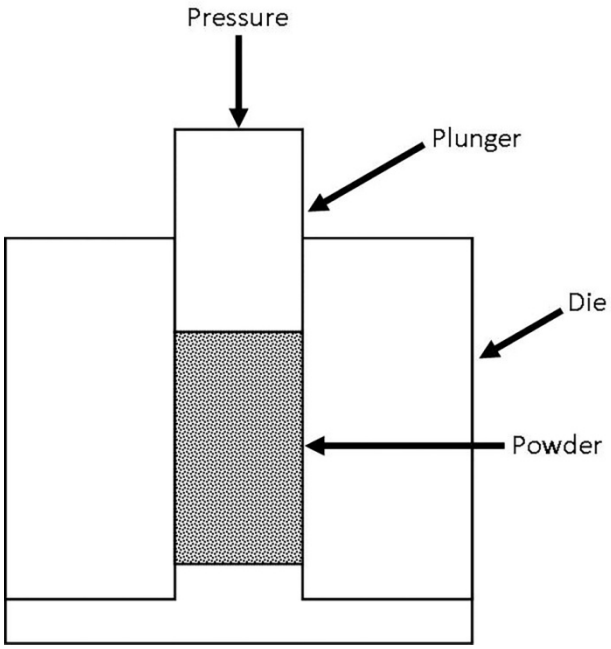

Fig.2.24: Uniaxial pressing.[42,43]

Process is finalized by ejecting the compacted body made from particulate solids (also known as green body, green compact or powder compact) from the pressing die. The compact now has the size and shape of the finished product (near net shape as it is known in the industry) with sufficient strength termed green strength.[44]At this stage the basic mechanism for particle bonding is interlocking.[45-47] Interlocking takes place when the powder particles (Fig. 2.25) become enmeshed due to plastic flow and generally as the compaction pressure increases so does the degree of interlocking.[48]

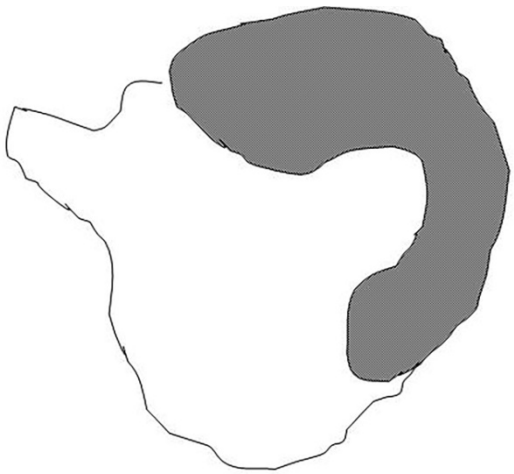

Fig 2.25: Pictorial representation of the interlocking binding mechanism of agglomeration.

Sintering is the heat treatment usually applied to green bodies after they have been compacted. The applied thermal energy densifies the specimen causing grain growth[49] and providing it with a permanent final strength that is generally superior to those of samples cut from melt grown ingots.[50]

2.5 Thermoelectric characterization

The thermoelectric characterization of thermoelectric specimens is performed using a *Z*-meter, an apparatus that measures the thermoelectric parameters of interest as a function of temperature.[51] The *Z*-meter consists of a hot-end and a cold-end or a heat sink in order to induce the ΔT required by the specimen to generate a voltage. Probes are usually fixed near the ends to measure their temperatures and

the ΔV generated and could be lowered or raised with precision in order to determine and adjust the vertical distance between them.

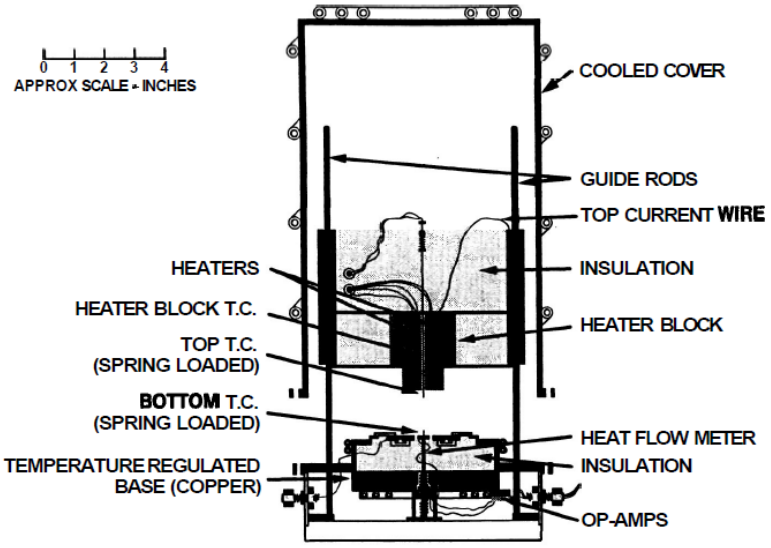

Fig. 2.26: *Z*-meter, a schematic representation.[51]

Chapter 3: Methodology

3.1 Unsintered uniaxial dry cold pressing

The UDCP method offers important advantages: small amounts of valuable research compounds are required to produce a powder compact (≈1 g); by means of a repeatable, consistent and safe procedure that uses inexpensive equipment. The dimensional control due to the well-defined cavity means that no mechanical post-pelletization processes or finishing are required, thus, the green bodies are ready to use or test immediately after pelletization.

High compaction pressures due to the hydraulic pressing equipment lead to typical green densities for compacted parts of 75–85% of their bulk density.[52] Excellent control of applied force and pressure allows repeatability and consistency in pelletized powders. Since the UDCP procedure used for this work did not involve agglomerating binders, there were no modifications induced of the electronic properties in the parent powder.

Due to the significant practical advantages that cold pressing has to offer when compared to other methods, it has already been considered and used before by other researchers as an alternate way to fabricate thermoelectrical specimens. [53–57] Please note, that in all of these cases sintering succeeded cold pressing.

Even if full-powder densification cannot be achieved by means of unsintered UDCP, unsintered compacts are a logical alternative considering that: (1) the thermoelectric figure of merit (Z) can be improved by reducing the lattice contribution to the thermal conductivity (λl) through scattering phonons on its multiple grain boundaries[58, 59] and (2) the strength provided by sintering is not necessary in this case, since test specimens will not be subjected to mechanical loads or stresses.

The present work documents for the first time the thermoelectrical characterization of unsintered UDCP Bi_2Te_3 and TiS_2. The relationship between the applied pressure and the achieved densification on the pellet is presented as well. A comparison was made between the specimens that had been prepared according to this procedure and their fully dense equivalents.

Two layered chalcogenides Bi_2Te_3 and TiS_2 with known physical and thermoelectric properties, Bi_2Te_3 –a semiconductor- and TiS_2 –a semimetal-[60-62] were selected to test and validate the UDCP method. Layered structures - also known as two-dimensional compounds- are ideal candidates for thermoelectric materials as they are bonded by weak Van de Walls forces, a feature that renders the crystal structure of the considered phase flexible enough to accommodate impurities. Impurities might be dopants, nano-particles, nano-domains or solid solution catalyzers that will optimize the thermoelectric properties.[63] In addition, theoretical calculations predict that a two-dimensional electronic structure enhances thermopower.[64]

Although TiS_2 is not a semiconductor and ideal thermoelectrics are semiconductors, TiS_2 is a layered compound that can be manipulated through bandgap engineering to obtain the desired properties. On other applications, field effect transistors (FET) based on layered compounds are promising because they can avoid the shorted-channel effect, which is one of the biggest obstacles for further miniaturization of semiconductors.[65,66]

Bi_2Te_3 is the best commercially available thermoelectric and it has been reported that TiS_2 can exhibit comparable thermopowers (S) to those of Bi_2Te_3.[67] In spite of the large thermopower generated by TiS_2, it has not been implemented on commercial applications due to its relatively large thermal conductivity[67] of 6.8 W/K m when compared[64] to 2.3 W/K m of Bi_2Te_3[68] which leads to a less efficient thermoelectric device. Most of this thermal conductivity comes from reducible lattice contribution.[67]

The Z-meter was calibrated using the standard specimens or standard reference material (SRM) from the National Institute of Standards (NIST) SRM 3451 for Seebeck coefficient and the SRM 8420 for electrical conductivity.

3.2 Equipment

A Hitachi TM-1000 Tabletop scanning electron microscope using backscattered electron imaging[69] at a fixed accelerating voltage of 15 kV was used to observe and document the morphology of powders before being pressed.

Fig. 3.1: Hitachi TM1000 tabletop SEM.[69]

Thermoelectric characterization of the specimens was performed using a *Z*-meter with a vertical probe-to-probe set distance of 3.81 mm:

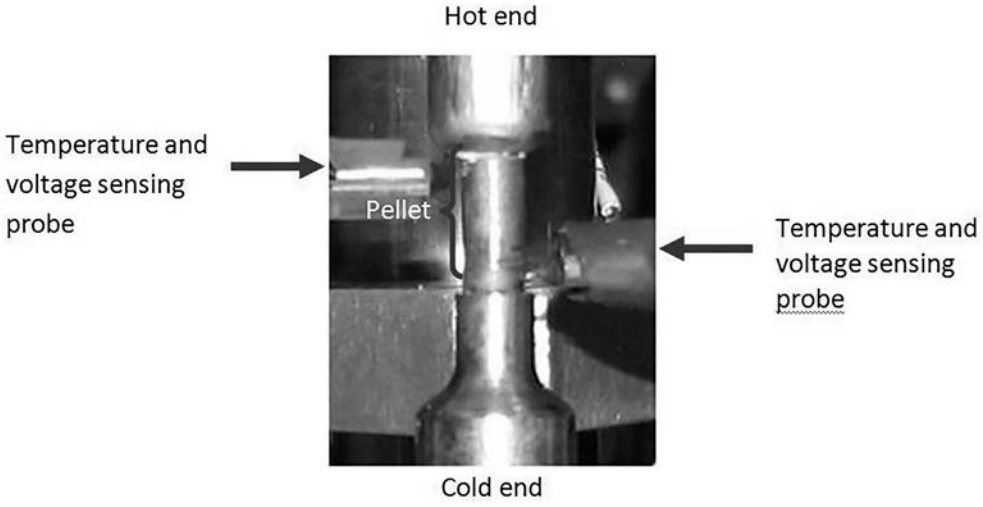

Figure 3.2: *Z*-meter and specimen set-up.

The electrical resistivity ρ was calculated by applying a voltage through the probes and measuring the electrical resistance *I*. The cross-sectional area *A* of the specimen was previously known as well as the distance *l* between the probes:

$$\rho = R\frac{A}{l}$$

Equation 3.1 Electrical resistivity

Please note that the Seebeck coefficient does not depend on the distance between the electrodes or on the thickness of the sample, this is due to the fact that the seebeck coefficient and the electric field share an identical length scale that vanishes in the final result.

The reference Bi_2Te_3 single crystal was bought from Marlow Industries. It was manufactured by the Bridgman process[70] and its properties conformed to the 'Standard Reference Material® Certificate No. 3451for Low Temperature Seebeck Coefficient Standard (10 K to 390 K)' issued by the National Institute of Standards & Technology.[71] The TiS_2 reference values used for comparison purposes were obtained from a single-crystal grown by the CVT method using I_2 transport.[72]

Crystalline Bi_2Te_3 powder was purchased from Sigma Aldrich, while the crystalline TiS_2 was provided by Dr Chianelli. The TiS_2 was synthesized by a CVT method using iodine as the transport agent, following the method as described by Thompson *et al*.[73]

A resistivity calibrating standard was used and the values generated were compared to its table values in order to adjust the data recording software accordingly. The properties of the aforementioned calibrating standard conformed to the 'National Bureau of Standards report of investigation research materials 8420 and 8421 electrolytic iron thermal conductivity (λ) and electrical resistivity (ρ) as a function of temperature from 2 to 1000 K.'[74]

Two cylindrical pressing die sets were used to develop and refine the pelletizing technique. A medium pressure die set, a heat treated steel 6 mm in diameter rated to 4 metric tons maximum load, and a high-pressure tungsten carbide die set 6.3 mm in diameter rated to 7 metric tons maximum load. A Carver C-3851 manual two column hydraulic bench top laboratory press with 12 ton capacity was used (Fig. 3.3) and after desired pressure was achieved, pellet was allowed a time of residence of 7 min at constant pressure to compensate for specimen elastic springback or expansion of compressed air.

Fig. 3.3 Hydraulic press and cylindrical die set.[75]

The density of the samples was calculated after measuring their weight with a high precision analytical balance and their length with a digital caliper. The relative densification was then determined by calculating the ratio between the specimen density and the bulk material density.

Chapter 4: Results and discussion

4.1 Unsintered uniaxial dry cold pressing

The following scanning electron images show the morphology of the parent powders before being pressed. The Bi_2Te_3 spherical particles and the TiS_2 successfully obtained nanolayers in the form of blossoming flowers:

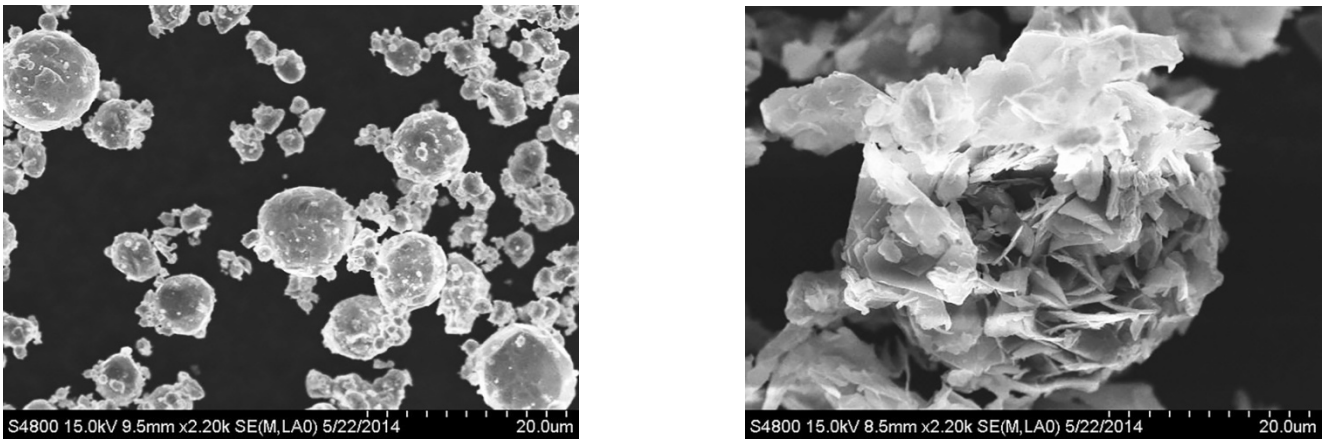

Fig. 4.1: *Left Image* Bi_2Te_3 powder SEM photomicrograph. Magnification 2,200X, *Right Image* TiS_2 powder SEM photomicrograph. Magnification 2,200X.

During pressing it was observed that for the applied pressure ranges (1.2–2.1 GPAs) an increase in pressure did not translate into an augmented densification. The limiting factor was atmospheric in nature as atmospheric gas is entrapped within pores as they are isolated (Table 1).[49]

Table 4.1: Specimen densification vs. applied pressure

Pellet diameter, mm	Pressure, GPAs	Relative densification, %
6	1.2	≈ 79.2
6	1.4	≈ 79.8
6.3	2.1	≈ 79.8

The following figures show TiS_2 pellet the as ejected:

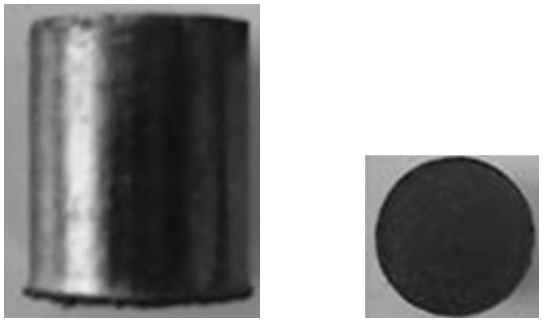

Fig. 4.2: *Left Image* TiS_2 Green compact side view, *Right Image* top view. Pictures is not to scale

The table below shows the values for the Seebeck coefficient and the electrical conductivity at 300 K for Bi_2Te_3 and TiS_2 both, uniaxially dry–cold pressed and single-crystal specimens compared side to side. Please note that for both compounds the sample's Seebeck coefficient is either identical or fairly close regardless the agglomerating method, while the electrical resistivity of the UDCP samples is significantly smaller (Table 2).

Table 4.2: Fully dense vs. UCDP thermoelectric properties

Compound	**Bi_2Te_3**		**TiS_2**	
Specimen	**Fully dense single crystal**	**UDCP**	**Fully dense polycrystal**	**UDCP**
Seebeck coefficient, μV/K	-231	-231	-153	-127
Electrical conductivity, S/m	100,000	4,065	61,350	2,134
Relative electrical conductivity		1		0.5

4.1.1 Relative conductivity

Of little use is an electrical conductivity comparison between single-crystal and UDCP specimens for the same compound. A more objective and meaningful approach is to compare the electrical conductivity of the UDCP experimental compound to the electrical conductivity of a UDCP Bi_2Te_3 reference sample. The resultant value has been termed relative electrical conductivity:

$$\sigma_r = \frac{\sigma_{exp}}{\sigma_{Bi_2Te_3}}$$

Equation 4.1: Relative electrical conductivity

Where σ_r is the relative electrical conductivity, σ_{exp} is the electrical conductivity of the UCDP experimental compound, σ_{Bi2Te3} is the electrical conductivity of UDCP Bi_2Te_3. If by default the electrical conductivity of UDCP Bi_2Te_3 is defined as 1, the relative electrical conductivity of UDCP TiS_2 is 0.5 and when the same method is applied to their single-crystal form σ_r is 0.6. Such results indicate that the relative electrical conductivity of an experimental compound might be used as a tool to predict the electrical conductivity in its fully dense condition.

4.2 Thermoelectric evaluation of other compounds

Following the successful evaluation of TiS_2 -a Transition Metal Chalcogenide or TMC-, the UCDP was extended to other TMCs with layered structures: $TaSe_2$, $ZrTe_2$, $TiSe_2$; to VS_4 -a TMC with a chain structure held together by Van der Walls- and to MoS_3 an amorphous TMC. Note that even if some materials show poor thermoelectric values they should not be ignored; since their electronic structure may be modified the same way that graphene is nowadays modified.

4.2.1 $TaSe_2$

$TaSe_2$ generated α= -11 μV/K and σ = 724,034 S/m; almost perfectly matching published results of α= -13 μV/K (76) and σ = 769,000 S/m (77). Even if the electrical conductivity of $TaSe_2$ is more than sevenfold that of Bi_2Te_3, its low Seebeck coefficient does not make it a promising thermoelectric in the as tested condition.

4.2.2 $ZrTe_2$,

Thermoelectric characterization of $ZrTe_2$ generated α= 351 μV/K and σ = 1,304 S/m. The $ZrTe_2$ used for this work exceeded the thermopower of Bi_2Te_3 (-231 μV/K) but its electrical conductivity was significantly smaller.

4.2.3 VS_4

Patronite (VS_4) -a chain-structured one dimensional tetrachalcogenide-[78] was the only sample that was not synthesized artificially; the mineral was provided by the Smithsonian and proceeded from Minas Ragra in Peru. To date, a systematic study of VS_4, including its bulk synthesis, properties and potential applications has not been performed owing to technical difficulties when trying to synthesize it making experimental data practically unavailable. [79] Thermoelectric characterization of patronite (VS_4) generated the following results α= 52 μV/K and σ = 0 S/m making it of no interest for thermoelectrical applications in its tested condition.

4.2.4 MoS_3

MoS_3 is an amorphous –chain structured- transition metal trichalcogenide with diamagnetic and semiconducting properties.[80,81] The list of applications for MoS_3 is extensive : as a cathode material in lithium batteries,[82] nanoparticle solid lubricant coating,[83] antifrictional and antiwear additive to lubricants,[84] and more rencently it is being explored as a photocatalytist for hydrogen evolution.[85,86] Despite the versatility of MoS_3, the thermoelectric characterization generated α= -247 μV/K and σ = 25 S/m deeming it of no interest for thermoelectrical applications in its tested condition.

4.2.5 $TiSe_2$

Initial (t_0) $TiSe_2$ thermoelectric measurements (α= -34039 μV/K and σ = 19 S/m) did not correspond to values[63] for pure $TiSe_2$ (α= -5 μV/K, σ = 91,743 S/m). Bulk $TiSe_2$ is a semimetal with poor thermoelectrical properties while the first measurements were typical of an insulator. Consecutive testing demonstrated that this performance was not consistent over time as $TiSe_2$ underwent an insulator to a semimetal transitional state due to the presence of Iodine. Iodine had remained in $TiSe_2$ as an

unexpected contaminant from material synthesis. Remanent Iodine is usually removed at the time specimens are sintered but since specimens used in these work were left in their green state this was not the case. The presence of Iodine was detected and documented via SEM and EDS.

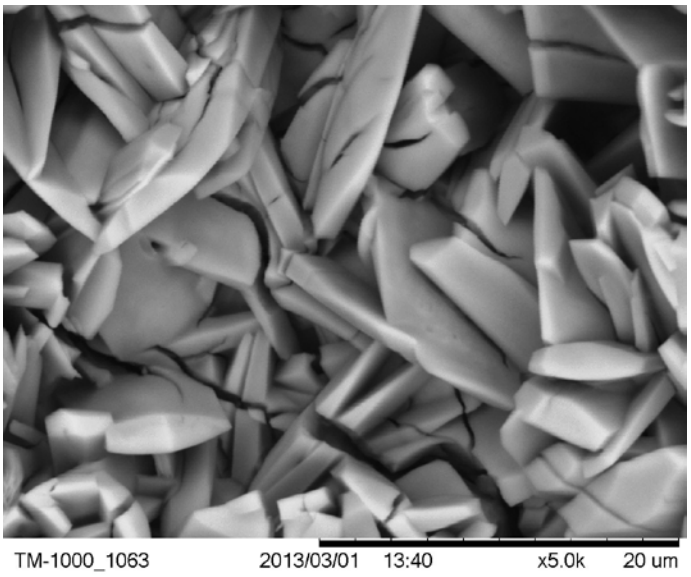

Fig. 4.3: I_2 crystals SEM photomicrograph. Magnification 5,000 X.

SEM was fitted with a SwiftED-TM Energy Dispersive (X-ray) Spectrometer[87](EDS) system, a silicon drift detector with a detection area of 30mm2 for semiquantitative chemical analysis. Preceding chemical analyses of the samples EDX detector was calibrated using copper standard reference tape.

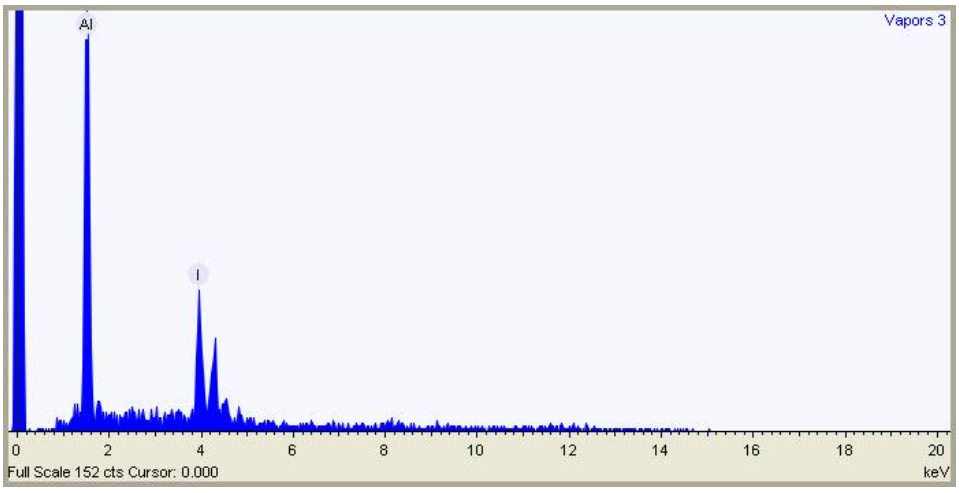

Fig. 4.4: I_2 crystals energy-dispersive X-ray spectroscopy.

Immediately after pelletization, the iodine concentration started to gradually decrease in the sample due to sublimation and gradually the induced insulator state became less prominent on the host material as thermoelectrical properties of an n-type semiconductor were observed. At $t \approx 319$ hours the transition from n-type to p-type took place.

At $t \approx 362$ the Seebeck coefficient reached a maximum of 4,579 μV/K and the electrical conductivity was 1.4 x10^6 S/m, characteristics consistent with a p-type semiconductor. Finally it was assumed that the material had reached steady state at $t \approx 387$ when $\alpha = 44$ μV/K, and $\sigma = 1.5 \times 10^6$ S/m.

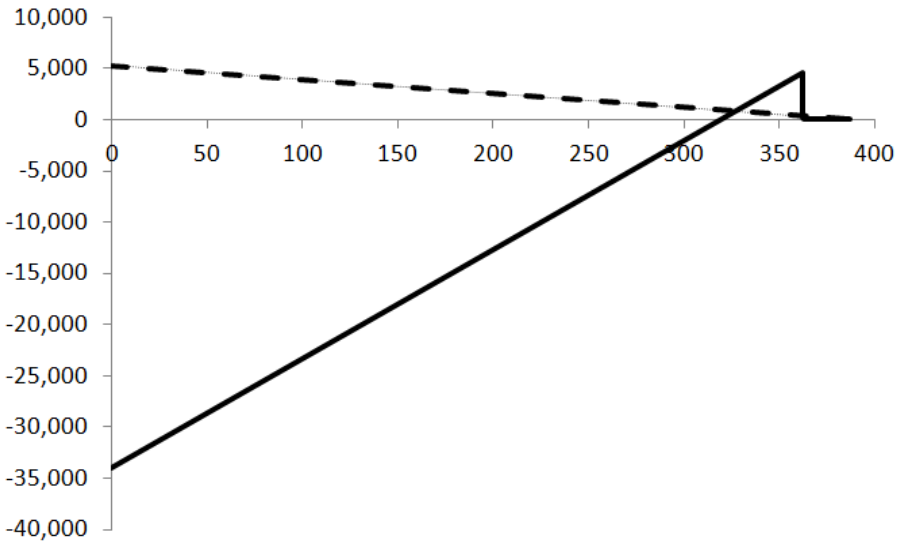

Fig. 4.5: α and σ of TiSe2-I2 doped in function of time.

The change of sign of the Seebeck coefficient presented here is not an isolated case, as semimetals switch their dominant type of conduction between N-type (electron-type) and P-type (hole-type) in function of temperature.[88] That is, for semimetals the sign of the Seebeck coefficient is temperature dependant, i.e. for $TiSe_2$ the S (300k) = -5 μV/K; S (700K) S= 47 μV/K.[63]

The insulator to semimetal transition observed in the experiments is not foreign to the $TiSe_2$ system. At the nanoscale and a given temperature ($T_{CDW} \approx 200$K), [89] single $TiSe_2$ layers are unstable

undergo a charge-density-wave (CDW) transition[90] inducing a Peierls distortion. In turn, the Peierls distortion originates a metal-to-insulator transition.[91]

The situation here is: 1) specimens were never submitted temperatures large enough (test was conducted at room temperature with a maximum Δt among probes of 2°C) to change the dominant type of conduction and 2) specimens were never taken to nanoscale. Being this the case, the results can only be attributed to the presence of iodine. $TiSe_2$ is extremely sensitive to imperfections, stoichiometrical deviations and impurity contamination –especially iodine- which adds a relatively large number of carriers strongly influencing the transport properties.[92]

Iodine has been used before as a doping agent to increase the electrical conductivity. The substrate was polyacetylene, and it was doped with iodine vapor in order to improve its electrical conductivity. The increase in conductivity after doping was 10 million times higher than before doping.[93]

Iodine has also been used before to invert the type of semiconductor. Goldsmid [94] and Dennis [95] doped Bi_2Te_3 (p-type) with iodine, causing the material to become n-type. They assumed they reached the optimal iodine doping when the maximum absolute thermoelectric power matched that of its undoped counterpart. The undoped Bi_2Te_3 (p-type) reached a maximum Seebeck coefficient of about 260 μV/K; while the iodine doped Bi_2Te_3 (n-type) reached a minimum of about -270 μV/K.[96]

Paul and Rawat used Iodine to improve the thermoelectric properties of PbTe. The addition of Iodine enhanced the power factor (PF) as well as the thermoelectric figure of merit (ZT) by tuning the position of the Fermi level by controlling electron density in the conduction band.[97]

4.3 $TiSe_2$ Materials Studio simulations

The Materials studio molecular simulation software was used in order to try to understand the mechanism that had led $TiSe_2$ to show such results. Two different types of simulations were performed, one simulating Iodine as a substitutional dopant and the other as an interstitial dopant. Both sets of simulations were performed with exactly the same amount of dopant in order to have an objective comparison.

Each peak on the simulations represents the electron states that are allowed states; those can be occupied by electrons as opposed to forbidden states. The x-axis represents the energy of that particular state in eVs and the y-axis represents the number of states available at that energy. The units on the y-axis are arbitrary units, scaled to whatever the simulation program determines to be a good relative me

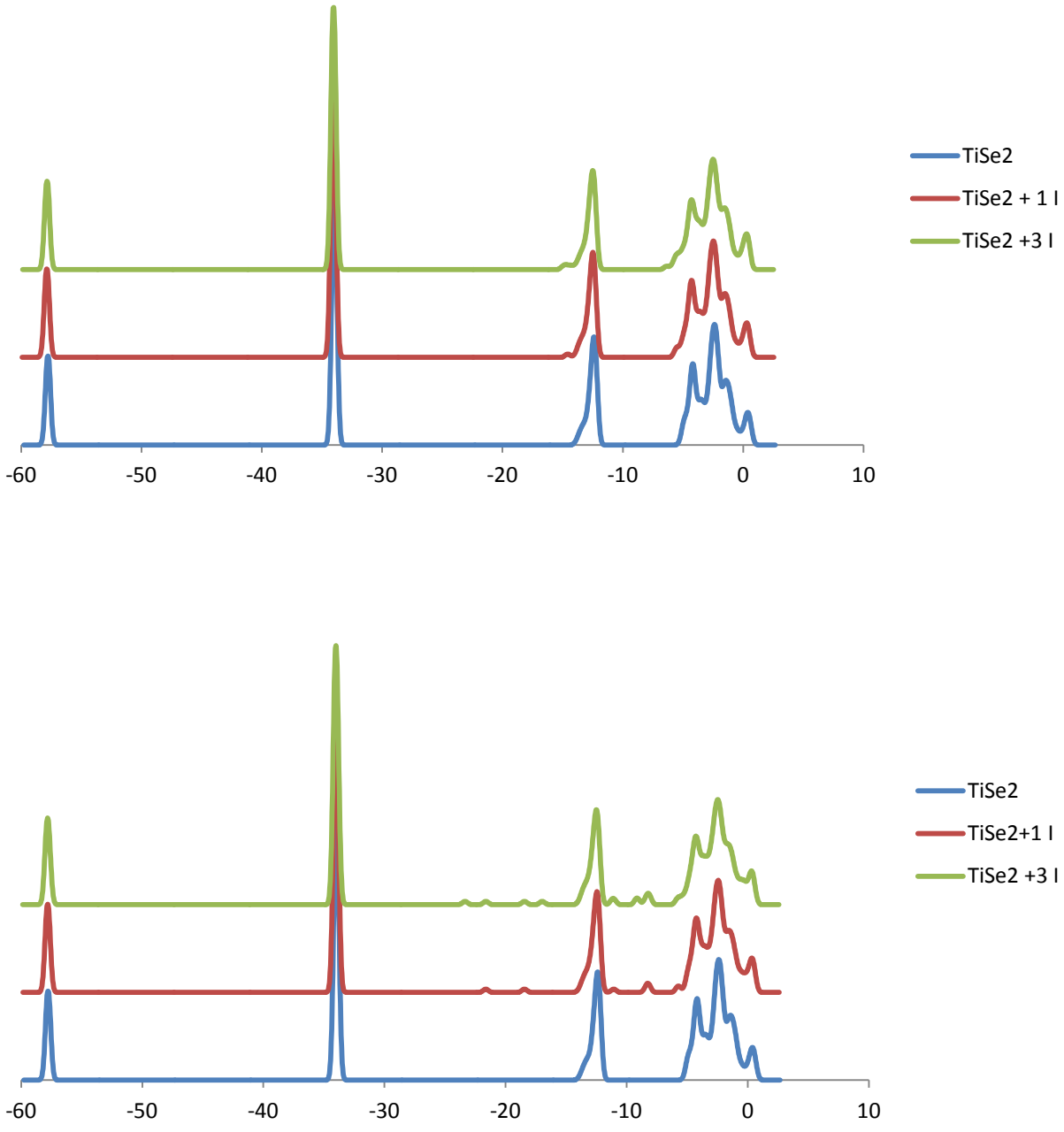

Fig. 4.7: TiSe2-I2 interstitially- doped, simulation.

The change in electrical conductivity that was experimentally observed was not reflected in the electronic density of states calculations either for substitutional doping or for interstitial doping (there should be a sharp increase of states near the Fermi level if this happens, since these are conduction states). The lack of computational correlation is most likely due to the unknown nature of iodine absorption in the bulk, resulting in the inability of the computational model to correlate with experiment.

Chapter 5: The Goldilocks Bandgap

A predictive model to theoretically preselect high performance thermoelectric compounds operating at room temperature was developed and validated. For this purpose the research path followed two leads: a) the possible relationship between the band gap of the material of interest and b) consideration of the intrinsic properties that define a thermoelectric.

In 1994 Sofo and Mahan theoretically derived the optimum band gap for semiconductors as thermoelectric materials[10] to be $6k_BT$ - $10k_BT$ corresponding to a band gap range of 0.15 - 0.25 eV, but at the end they did not correlate the theory with operative materials. Later, in 2008 Snyder and Toberer (S&T) developed a model solely based on Bi_2Te_3 that shows the relationship between α, σ, k, PF, and the figure of merit in function of the carrier concentration[11] and state that good thermoelectric materials are typically semiconductors with a carrier concentration between 10^{19} and 10^{21} carriers per cm^3. The graph below shows an improved version of the S&T model as well as the specifics corresponding to each type of material:

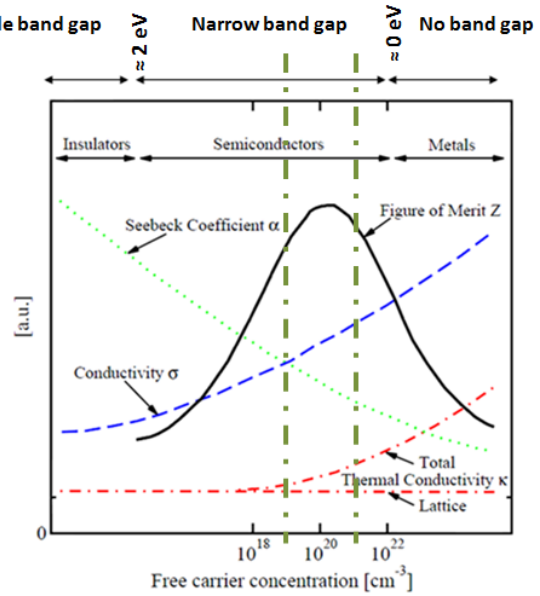

	Insulators	Semiconductors	Metals
α(μV/K)	≈ 1,000	≈ 200	≈ 5
σ (S/m)	≈ 10^{-10}	≈ 10^5	≈ 10^7
k (W/m·K)	0.1 - 1	1 -100	10 -1,000
zT	10^{-14}	0.1 - 1.0	10^{-3}

Fig. 5.1: Intrinsic property values for insulators, semiconductors and metals.[98]

The work presented here validates for the first time the results of S&M's with known thermoelectric materials and their empirical data:

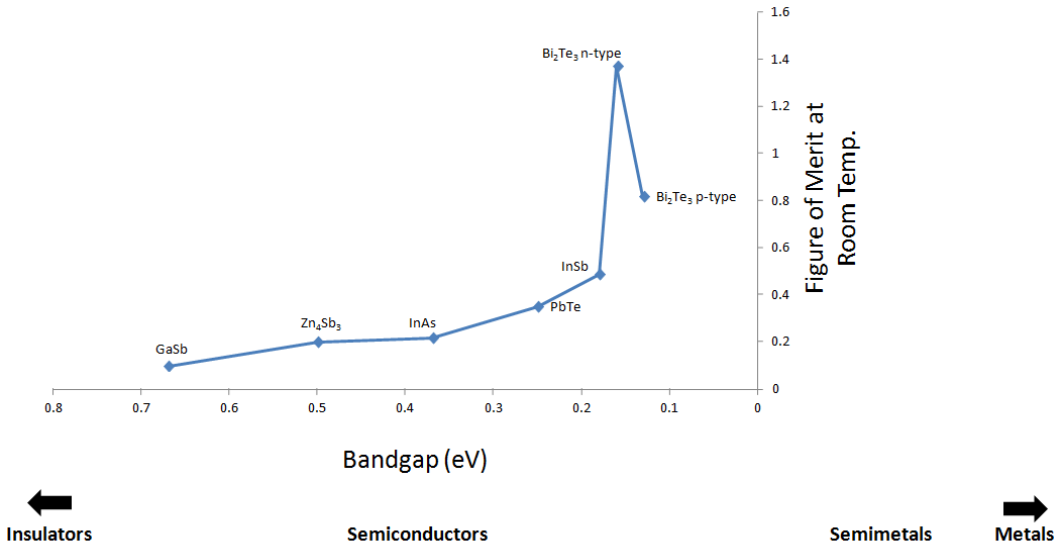

Fig. 5.2: Bandgap vs. *z* for various compounds, empirical data.

The model of ST's has been expanded to include materials of thermoelectric interest other than Bi_2Te_3 and integrated to SM's theoretical derivation:

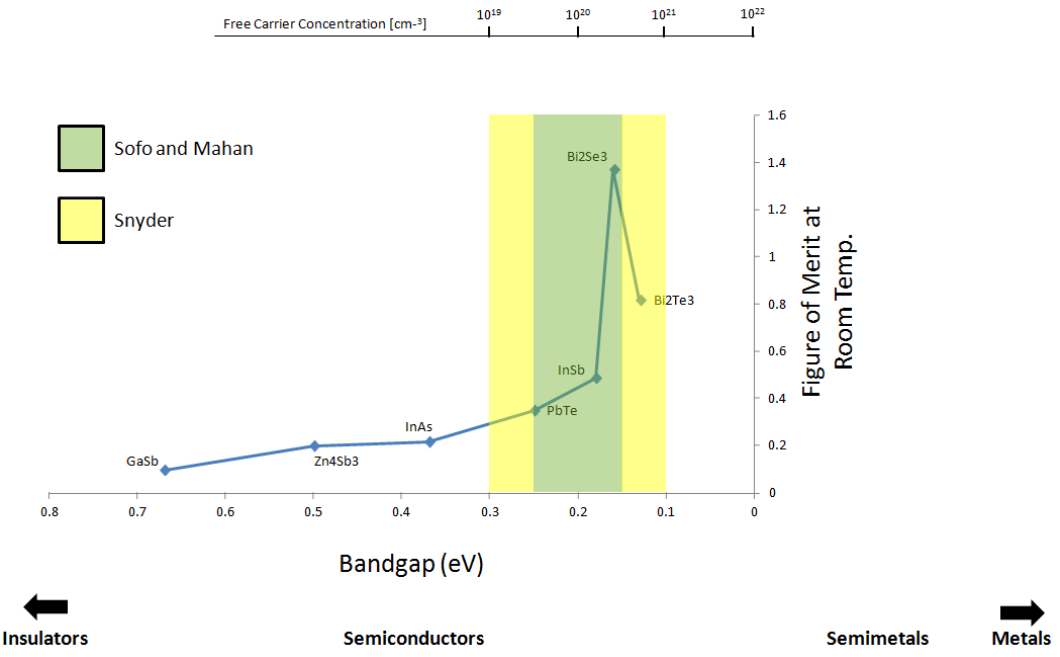

Fig. 5.3: Bandgap vs. z for various compounds with respect to theoretical predictions

The result of correlating the band gap with the free carrier concentration, indicates that SM's optimal band gap might be slightly enlarged from 0.15 – 0.25 eV to 0.1 - 0.3 eV. Moreover, new work by Goldsmid[99] states a material that fulfills the correct conditions might have a figure of Merit (zT) ≈ 6, breaking with the paradigm that figures of merit above 2 for room temperature thermoelectric materials might not be achievable.

The thermoelectric characterization results of the $TiSe_2$ demonstrate that even if the material has its bang gap off the optimal semiconducting limits to be considered as an efficient thermoelectric, it can be highly doped to engineer its band gap at will, and augment the free carrier concentration to make it an interesting material.

Chapter 6: Conclusions and final thoughts

6.1 UDCP

Unsyntered uniaxial dry cold pressing (UDCP) was developed as a new alternate way to agglomerate materials for thermoelectric evaluation. The method was tested and validated using the thermoelectric compound of reference Bi_2Te_3 and TiS_2. The concept of relative electrical conductivity was developed as a comparative tool among specimens agglomerated by the same method and with roughly the same densification.

The UDCP agglomerating method was extended to other TMCs with layered structures: $TaSe_2$, $ZrTe_2$, $TiSe_2$; to VS_4 -a TMC with a chain structure held together by Van der Walls- and to MoS_3 an amorphous. The UDCP agglomerating method was once again validated when thermoelectric evaluation of UDCP $TaSe_2$ matched perfectly published results.

Finally, the limiting factor for densification was atmospheric in nature as atmospheric gas is entrapped within pores as they are isolated. If higher densifications are desired, a modification to the UDCP method is suggested. The method can be upgraded if performed under a vacuum using an oil-free press remotely controlled like the one shown below:

Fig. 6.1: Electric scissor car jack.

6.2 $TiSe_2$

Of all the compounds evaluated, only $TiSe_2$ generated interesting results. $TiSe_2$ was doped with I_2 inducing a temporary insulator condition while observing improved thermoelectric properties. The presence of Iodine was verified via electron microscopy and EDS. TiSe2 doped with Iodine at various concentrations deserves an in-depth analysis.

6.3 The Goldilocks bandgap

A predictive method was developed, a method to preselect potentially good thermoelectric materials based on their bandgap. Such predictive method validated for the first time with empirical data, models developed before based on ab initio first principles. The optimal material should have bandgap should be within the 0.1 - 0.3 eV range.

6.3.1 Proposed Compounds

Based on Goldilocks bandgap and work performed previously by Lebègue *et al.*[13] the following list of compounds is proposed for future research:

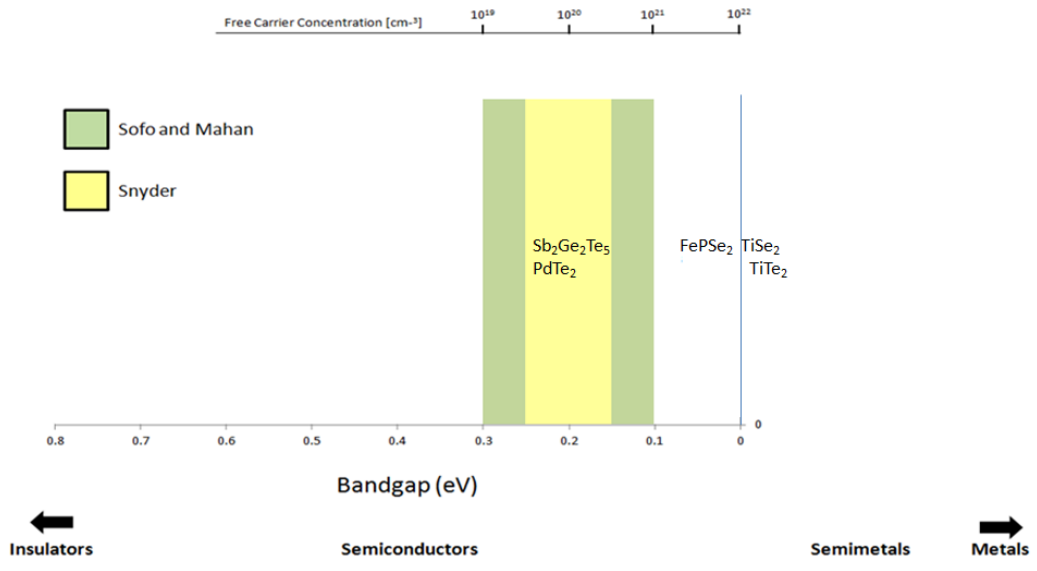

Fig. 6.2: Proposed compounds and their location in the Goldilocks

Table 6.1: List of proposed compounds

Compound	Notes
$TiSe_2$	To test doped with iodine at different concentrations
$Sb_2Ge_2Te_5$	0.2 eV band gap
$PdTe_2$	0.2 eV band gap
$FePSe_3$	0.05 eV band gap
TiTe2	To test doped to improve thermoelectric properties.

6.4 Refined PF, Z and ZT equations.

Although the equation to derive the dimensionless figure of merit (zT) is highly practical due to its simplicity it does not describe accurately its dependence on the thermoelectric intrinsic properties. The figure of merit is described as a parabola by the quadratic function while experimental data follows a Gaussian distribution.

$$zT = \frac{\alpha^2 \sigma T}{k}$$

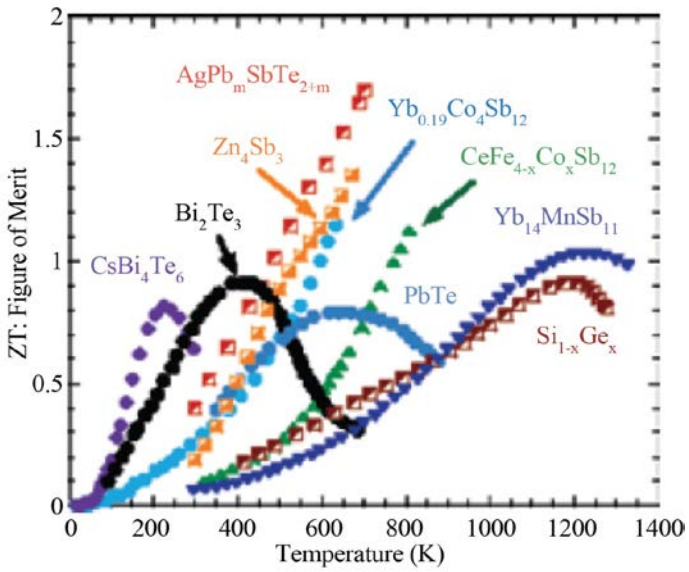

Fig. 6.3. *Left Image* equation for dimensionless figure of merit, *Right Image* experimental data for various thermoelectric compounds.[100]

The quadratic function and the Gaussian distribution share the same vertices nevertheless the difference of the areas under the curves is a significant one in order to be neglected.

$$zT = \frac{T}{k\sigma\sqrt{2\pi}}(e)^{\alpha^2}$$

$$zT = \frac{\alpha^2 \sigma\, T}{k}$$

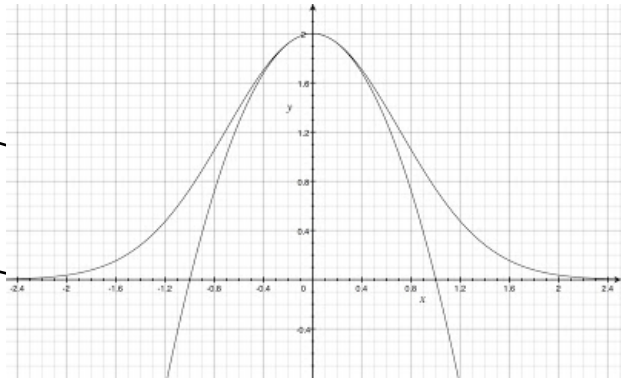

Fig. 6.4. Difference between the Quadratic function and the Gaussian distribution.

The refined equation can be applied to accurately describe experimental results or for predictive purposes either for single compounds or for a range a materials without the risk of potentially excluding data or materials of interest. In a similar manner, the figure of merit and the power factor can be calculated.

$$zT = \frac{T}{k\sigma\sqrt{2\pi}}(e)^{\alpha^2}, \qquad z = \frac{1}{k\sigma\sqrt{2\pi}}(e)^{\alpha^2}, \qquad PF = \frac{1}{\sigma\sqrt{2\pi}}(e)^{\alpha^2}$$

Equation 6.1:: From left to right refined equations for the dimensionless figure of merit, figure of merit and power factor following a Gaussian distribution.

References

1. https://en.wikipedia.org/wiki/Thomas_Johann_Seebeck
2. http://global.britannica.com/biography/Jean-Charles-Athanase-Peltier
3. T.J. Seebeck, Proc. Prussian Acad. Sci. (1822) 265–373.
4. E. Altenkirch, Phys. Zeitschrift 10 (1909) 560–580.
5. E. Altenkirch, Phys. Zeitschrift 12 (1911) 920–924.
6. M. V. Vedernikov and E. K. Iordanishvili "A. F. Ioffe and origin of modern semiconductor thermoelectric energy conversion" 17th Int. Conf. on Thermoelectrics vol 1, pp 37–42 (1998); A. F. Ioffe "Semiconductor Thermoelements and Thermoelectric Cooling"
7. H.J. Goldsmid, R.W. Douglas, British J. Appl. Phys. 5 (11) (1954) 386–390.
8. R.P. Chasmar, R. Stratton, J. Electron. Control 7 (1959) 52–72.
9. R. Simon, J. Appl. Phys. 33 (5) (1962) 1830–1841.
10. J.O. Sofo, G.D. Mahan, Phys. Rev. B 49 (7) (1994) 4565–4570.
11. Snyder, G. J.; Toberer, E. S. Nat. Mater. 2008 , 7, 105.
12. Goldsmid, H. J. "Improving the Power Factor and the Role of Impurity Bands." *Journal of electronic materials* 42.7 (2013): 1482-1489.
13. S. Lebègue, T. Björkman, M. Klintenberg, R. M. Nieminen, and O. Eriksson, Two-Dimensional Materials from Data Filtering and Ab Initio Calculations, Phys. Rev. X 3, 031002 (2013).
14. S. Joel: 'The cool TEC pad', Senior design fall 2012 final report, Wichita State University, USA, December 2012, available at http://cratel.wichita.edu/blogs/eecsseniordesignfall2012spring2013/2012/12/10/out-of-timeprototype-ii-final-report-cool-tec/ (accessed 3 October 2015).
15. http://oldradio.onego.ru/ARTICLES/RADIO/tgk.htm
16. http://www.roachman.com/thermic/
17. http://www.natureinterface.com/e/ni03/P045-049/
18. http://www.nasa.gov/centers/ames/research/technology-onepagers/human_devices.html
19. http://www.kelk.co.jp/english/useful/netsuden3.html

20. Free Speech, Internet, http://www.pbs.org/newshour/bradlee/background_security.html
21. http://sse.jpl.nasa.gov/scitech/display.cfm?ST_ID=2149
22. NASA Voyager Mission, http://voyager.jpl.nasa.gov/spacecraft/instruments_rtg.html
23. Advanced Stirling Radioisotope Generator Development. Richardson and Chan. Department of Energy and Lockheed Martin Space Systems Company.
24. http://en.wikipedia.org/wiki/Radioisotope_thermoelectric_generator#cite_note-20
25. http://inhabitat.com/world%E2%80%99s-first-positive-energy-building-planned-for-masdar/
26. http://www.kelk.co.jp/english/useful/netsuden4.html
27. Testing an automobile exhaust thermoelectric generator in a light truck. Thacher, Helenbrook, Karri, and Richter. University Press, Potsdam, New York, USA
28. http://www.themotorreport.com.au/19610/vw-and-bmw-dabble-in-thermoelectric-generators
29. Snyder, G. J.; Toberer, E. S. Nat. Mater. 2008 , 7, 105.
30. http://www.ieap.uni-kiel.de/surface/ag-kipp/epitaxy/cvt.htm
31. M. Binnewies, R. Glaum, M. Schmidt, P. Schmidt, Z. Anorg. Allg. Chem. 2013, 639, 219–229.
32. Handbook of Electronic and Photonic Materials by S. Kasap, P.Capper, Part B | 16.3, 2007. ISBN: 978 0 387 26059 4
33. A. Claude et al," Crystal Growth of Napthalene (C10H8) crystals using bridgemann-stockbarger technique" Arch. Phy. Res., 2012, 3 (4):309-314
34. Internet reference: www.mtixtl.com/xtlflyers/bridgman.doc Last accessed July 8th 2013
35. Handbook of Electronic and Photonic Materials by S. Kasap, P.Capper, Bulk Crystal Growth – Methods and Materials 12.3 Materials Grown p.248, 2007. ISBN: 978 0 387 26059 4
36. Bridgman Stockbarger technique WIKIPEDIA
37. Introduction to Thermoelectricity, H. Julian Goldsmid. p. 100. ISBN 978-3-642-00715-6
38. Fundamentals of Semiconductors, Physics and Materials Properties. ISBN 3-540-25470-6. Peter Y. Yu Manuel Cardona, pp 6,7
39. http://aam.mathematik.uni-freiburg.de/IAM/homepages/alfred/BSSBBDK.html
40. J. C. Brice: Crystal Growth Processes (Blackie, London 1986)

41. D.R. Lovett, Semimetals & Narrow-Bandgap Semiconductors, Pion Ltd., London, p. 30 (1977).
42. G. S. Nolas, H. Goldsmid and J. Sharp: 'Thermoelectrics: basic principles and new materials developments', 1st edn, Chap. 5, 'Review of established materials and devices', 130; 2001, Germany, Springer.
43. B. L. Ferguson and R. M. German: 'Powder shaping and consolidation technologies', in 'ASM handbook', 10th edn, Vol. 7, 'Powder metal technologies and applications', (ed. P. W.Lee *et al.*), 732–734; 1998, Materials Park, OH, ASM International.
44. S. Lampman: 'Compressibility and compactibility of metal powders', in 'ASM handbook', 10th edn, Vol. 7, 'Powder metal technologies and applications', (ed. P. W.Lee *et al.*), 716; 1998, Materials Park, OH, ASM International.
45. C. Orr: 'Particulate technology', 1st edn, 421, 1966, New York, NY:Macmillan Company.
46. B. B. Morgan: Brit. Coal Util. Res. Ass. Monthly Bull., Apr. 1961, 25, 125–137.
47. H. Rumpf: 'The strength of granules and agglomerates', in 'Agglomeration'(ed. W. A. Knepper), 379–419;1962, New York, NY: John Wiley.
48. S. Clyens and W. Johnson: Mater. Sci. Eng., Oct. 1977, 30, (2), 121–139.
49. S. Kang: 'Sintering, Densification, Grain Growth & Microstructure', 1st edn, Chap. 1, 7, 2004, Oxford: Elsevier.
50. H. J. Goldsmid: 'Electronic refrigeration', 1st edn, Chap. 6, 'Production of materials', 161; 1986, London, Pion
51. H. H. Woodbury, L. M. Levinson and R. S. Lewandowski: 'Z-meters, in 'CRC handbook of thermoelectrics', 1st edn, (ed. D. M. Rowe), secn. c, part 17, 181, 1995, Boca Raton, FL, CRC press.
52. B. L. Ferguson and R. M. German: 'Powder shaping and consolidation technologies', in 'ASM handbook', 10th edn, Vol. 7, 'Powder metal technologies and applications', (ed. P. W.Lee *et al.*), 732–734; 1998,Materials Park, OH, ASM International.

53. H. J. Goldsmid: ‘Electronic refrigeration’, 1st edn, Chap. 6, ‘Productionof materials’, 161; 1986, London, Pion.
54. J. Navrátil, Z. Starý and T. Plecháček: *Mater. Res. Bull.*, Dec. 1996, **31**,(12), 1559–1566.
55. J. L. Cui: *J. Alloy Compd.*, May 2006, **415**, (1–2), 216–219.
56. Z. Li, G. L. Zhao, P. Zhang, S. Guo and J. Tang: *Mater. Sci. Appl.*, 2012,**3**, 833–837.
57. Y. Gelbstein, Z. Dashevsky and M. P. Dariel: *Physica B*, June 2005, **363**,(1–4), 196–205.
58. G. S. Nolas, H. Goldsmid and J. Sharp: ‘Thermoelectrics: basic principles and new materials developments’, 1st edn, Chap. 5, ‘Review of established materials and devices’, 130; 2001, Germany, Springer.
59. D. M. Rowe and C. M. Bhandari: *Appl. Energy*, Sept. 1980, **6**, (5), 329–401.
60. A. H. Thompson, K. R. Pisharody, and R. F. Koehler, Jr., Phys. Rev. Lett., 29, 163 (1972).
61. A. H. Thompson, F. R. Gamble, and C. R. Symon, Mat. Res. Bull., 10, 915 (1975).
62. Electronic structure of TiS_2 and its electric transport properties under high pressure Liu, Yang/ Electronic structure of 1*T*-TiS_2 Sangeeta Sharma, Tashi Nautiyal, G. S. Singh, and S. Auluck
63. F. Gascoin, N. Raghavendra, E. Guilmeau, and Y. Breard, J. Alloys Compd. 521, 121 (2012).
64. L.D. Hicks and M.S. Dresselhaus, Phys. Rev. B 47, 12 727 (1993).
65. W. Zhang, Z. Huang, W. Zhang, and Y. Li, Nano Res. 7, 1731 (2014).
66. Han Liu, Adam T. Neal, and Peide D. Ye. ACS Nano, 6(10):8563–8569, 2012.
67. H. Imai, Y. Shimakawa, and Y. Kubo, Phys. Rev. B 64, 241104 (2001).
68. Tritt, Terry M., ed. Thermal conductivity: theory, properties, and applications. Springer, 2004.
69. ‘Hitachi TM1000 tabletop scanning electron microscope product brochure’, Hitachi High-Technologies Corporation, Tokyo, Japan, August 2007, available at https://www.kth.se/polopoly_fs/1.143167!/Menu/general/column-content/attachment/TM1000.pdf (accessed 3 October2015).
70. ‘Thermoelectric materials & manufacturing’, II-VI Marlow, Dallas, TX, USA, available at: http://www.marlow.com/resources/knowledgebase/vi-process-from-concept-to-completion/c-manufacturing-capability/1-thermoelectric-materials.html (accessed 3 October 2015).

71. D. L. Kaiser and R. L. Watters: ‘Low- temperature seebeck coefficient standard (10 K to 390)’, NIST SRM 3451, 2011, National Institute of Standards, Gaithersburg, USA.
72. 10. C. A. Kukkonen, W. J. Kaiser, E. M. Logothetis, B. J. Blumenstock, P.A. Schroeder and S. P. Faile, R. Colella and J. Gambold: *Phys. Rev. B*,Aug. 1981, **24**, (4), 1691–1709.
73. A. H. Thompson, F. R. Gamble and C. R. Symon: *Mat. Res. Bull.*, Sept.1975, **10**, (9), 915–919.
74. J. G. Hust and A. B. Lankford: ‘Standard reference materials: thermal conductivity and electrical resistivity as a function of temperature from 2 to 1000 K- Electrolytic Iron-’, NIST SRM 8420/8421, 1984, Gaithersburg,MD, USA, National Bureau of Standards.
75. ‘Cylindrical dies’, Across International, Livingston, NJ, USA, available at http://www.acrossinternational.com/Cylindrical-Dies_c22.htm (accessed 3 October 2015).
76. L.H. Brixner, J. Inorg. Nucl. Chem. 24 (1962) 257.
77. M. H. Van Maaren and G. M. Schaffer, Phys. Letters 24A, 645 (1967).
78. Ratha, S., Marri, S. R., Lanzillo, N. A., Moshkalev, S., Nayak, S. K., Behera, J. N., & Rout, C. S. (2015). Supercapacitors based on patronite–reduced graphene oxide hybrids: experimental and theoretical insights. Journal of Materials Chemistry A, 3(37), 18874-18881.
79. Rout, C.S.; Kim, B.H.; Xu, X.; Cho, J.P.; Shin, H.S. J. Am. Chem. Soc. 2013, 135, 8720−8725.
80. Gopalakrishnan, J., and K. S. Nanjundaswamy. "Transition metal chalcogenides exhibiting quasi-one-dimensional behaviour." Bulletin of Materials Science 5.3-4 (1983): 287-306.
81. Liang, K.S.; DeNeufville, J.P.; Jacobson, A.J.; Chianelli, R.R. J. Non-Cryst. Solids 1980, 35-36, 1249.
82. Liang, K. S.; Cramer, S. P.; Johnston, D. C.; Chang, C. H.; Jacobson, A. J.;. Deneufville, J. P.; Chianelli, R. R. J. Non-Cryst. Solids 1980, 42, 345.
83. Lince, Jeffrey R., et al. "Tribochemistry of MoS3 Nanoparticle Coatings." Tribology Letters 53.3 (2014): 543-554.
84. Parenago, O. P., et al. "Antifriction and antiwear properties of molybdenum sulfides nanosized particles synthesized using nitrogen containing ionic liquids." Scientific problems of machines operation and maintenance 1 (161). Polish Tribological Society, 2010.

85. M. L. Tang, D. C. Grauer, B. Lassalle-Kaiser, V. K. Yachandra, L. Amirav, J. R. Long, J. Yano and A. P. Alivisatos, Angew. Chem., Int. Ed., 2011, 50, 10203–10207.
86. W. Zhang, T. H. Zhou, J. W. Zheng, J. D. Hong, Y. X. Pan, R. Xu, ChemSusChem 2015,8 (8), 1464–1471. DOI: 10.1002/cssc.201500067
87. SwiftED-TM Energy Dispersive X-ray Spectrometer product brochure. Hitachi High-Technologies Corporation. http://www.hitachi-hitec.com
88. Ishiwata, S., Shiomi, Y., Lee, J. S., Bahramy, M. S., Suzuki, T., Uchida, M., Arita, R., Taguchi, Y. & Tokura, Y. Extremely high electron mobility in a phonon-glass semimetal. *Nature Materials* **12,** 512–517 (2013).
89. Hilderbrand, B.; Didiot, C.; Novello, A. M.; Monney, G.; Scarfato, A.; Ubaldini, A.; Berger, H.; Bowler, D. R.; Renner, C.; Aebi, P. Doping Nature of Native Defects in 1T-TiSe2. Phys. Rev. Lett. 2014, 112, 197001.
90. Bhatt, R.; Bhattacharya, S.; Basu, R.; Ahmad, S.; Chauhan, a. K.; Okram, G. S.; Bhatt, P.; Roy, M.; Navaneethan, M.; Hayakawa, Y.; et al. Enhanced Thermoelectric Properties of Selenium-Deficient Layered TiSe2−x: A Charge-Density-Wave Material. ACS Appl. Mater. Interfaces 2014, 6, 18619−18625.
91. http://nanowiz.tripod.com/lowdim/peierls.htm, 1998–2008 Dmitri Petrovykh. Updated 28-Dec-2008.
92. Di Salvo, F. J., Moncton, D. E. & Waszczak, J. V. Electronic properties and superlattice formation in the semimetal TiSe2.Phys. Rev. B14, 4321–4328 (1976).
93. http://www.chemheritage.org/discover/online-resources/chemistry-in-history/themes/microelectronics-and-nanotechnology/macdiarmid-heeger-shirakawa.aspx
94. Goldsmid, H. J. 1957. The Thermal Conductivity, Electrical Conductivity, and Thermal Power of Bismuth Telluride. Ph. D. Thesis, University of London. (Proc. Phys. Soc. (London), in press.)
95. Jane H. Dennis, Anisotropy of Thermoelectric Power in Bismuth Telluride, Ph. D. Thesis, Department of Electrical Engineering, MIT (Technical Report 377, Research Laboratory of Electronics, MIT).

96. Nolas, G. S.; Sharp, J.; Goldsmid, H. J. Thermoelectrics: Basic Principles and New Materials Developments; Springer: Berlin, 2001

97. B. Paul, P.K. Rawat, and P. Banerji, Appl. Phys. Lett. 98, 262101 (2011).

98. J. P. Fleurial, « Design and discovery of highly efficient thermoelectric materials », presented at the 9th CIMTECH-World ceramics congress and forum on new materials, Florence , Italy (14/06/1998), vol. 24, p. 733-744.

99. Goldsmid, H. J. "Improving the Power Factor and the Role of Impurity Bands." *Journal of electronic materials* 42.7 (2013): 1482-1489.

100. T. Jarman, E. Khalil, E. Khalaf, Energy analyses of thermoelectric renewable energy sources, Open J. Energy Efficiency 2 (2013) 143–153, http://dx.doi. org/10.4236/ojee.2013.24019.

Vita

Hugo Lopez earned his Bachelor of Engineering degree in Metallurgical and Materials Engineering from UTEP in 2003 while doing research on impact crater characterization under the supervision of Dr. Murr. He coauthored the article: “Microbands and microtwins associated with impact craters in copper and brass targets: the role of stacking fault energy.”

While working as a Materials Engineer at the Delphi Mexico Technical Center Material’s Lab he decided to obtain a Masters in Materials Science and Engineering. In 2008 he entered the program and in 2010 he received his Master of Science from UTEP. He performed research on electron beam melted titanium alloys under the supervision of Dr. Murr and coauthored the article: “Next-generation biomedical implants using additive manufacturing of complex, cellular and functional mesh arrays.”

After obtaining his Masters degree he immediately joined the doctoral program in Materials Science & Engineering at UTEP. Under the supervision of Dr. Chianelli he did research on novel Thermoelectric materials and partial results were published on the article entitled “Uniaxial dry cold pressing as a rapid specimen fabrication technique aimed at dynamizing the screening of materials of Thermoelectric interest: The specific case of Bi2Te3 and TiS2.”

Dr. Lopez was the recipient of numerous honors and awards including The Chihuahua Scholarship and the Delphi’s excellence award. He is currently a member of Tau Beta Pi, The Engineering Honor Society and Alpha Sigma Mu the Metallurgical and Materials Engineering honor society.

Permanent address: 4 Rue Leonhard Euler

94000, Créteil, France

This dissertation was typed by Hugo Francisco Lopez Lopez De Cardenas.